Biofouling, 2015
Vol. 31, Nos. 9–10, 759–773, http://dx.doi.org/10.1080/08927014.2015.1108407

Taylor & Francis
Taylor & Francis Group

Impact of diatomaceous biofilms on the frictional drag of fouling-release coatings

M. P. Schultz[a]*, J. M. Walker[b], C. N. Steppe[c] and K. A. Flack[d]

[a]*Department of Naval Architecture and Ocean Engineering, United States Naval Academy, Annapolis, USA;* [b]*National Centre for Maritime Engineering and Hydrodynamics, Australian Maritime College, University of Tasmania, Launceston, Australia;* [c]*Department of Oceanography, United States Naval Academy, Annapolis, USA;* [d]*Department of Mechanical Engineering, United States Naval Academy, Annapolis, USA*

(*Received 17 July 2015; accepted 9 October 2015*)

Skin-friction results are presented for fouling-release (FR) hull coatings in the unexposed, clean condition and after dynamic exposure to diatomaceous biofilms for 3 and 6 months. The experiments were conducted in a fully developed turbulent channel flow facility spanning a wide Reynolds number range. The results show that the clean FR coatings tested were hydraulically smooth over much of the Reynolds number range. Biofilms, however, resulted in an increase in skin-friction of up to 70%. The roughness functions for the biofilm-covered surfaces did not display universal behavior, but instead varied with the percentage coverage by the biofilm. The effect of the biofilm was observed to scale with its mean thickness and the square root of the percentage coverage. A new effective roughness length scale (k_{eff}) for biofilms based on these parameters is proposed. Boundary layer similarity-law scaling is used to predict the impact of these biofilms on the required shaft power for a mid-sized naval surface combatant at cruising speed. The increase in power is estimated to be between 1.5% and 10.1% depending on the biofilm thickness and percentage coverage.

Keywords: drag; powering; biofilms; biofouling; roughness; fouling-release coatings

Downloaded by [US Naval Academy] at 05:19 14 December 2015

Introduction

The consequences of marine biofouling are significant and far-reaching. One such outcome is the increase in hull roughness on ships due to the settlement and growth of biofouling organisms. This increased roughness elevates frictional drag, which in turn increases fuel consumption and decreases vessel range and speed (eg Kempf 1937; Lewthwaite et al. 1985; Leer-Andersen & Larsson 2003; Townsin 2003; Schultz 2007). These outcomes also generate a significant economic impact. For example, an economic analysis of US Navy destroyers places the overall cost associated with hull fouling at ~ $1 million per ship per year (Schultz et al. 2011).

A great deal of research has focussed on understanding the effects of biofouling on ship drag and powering. A review of this work is given by Townsin (2003), and a primary conclusion of this paper is that the impact of calcareous macrofouling (eg barnacles and oysters) is much better understood than for soft fouling (eg bacteria, micro- and macroalgae). There are several possible reasons for this. First, biofilms are complex assemblages of diverse organisms ranging from bacteria to diatoms and algae. This makes them highly variable in density, height and other parameters that affect their 'effective' roughness height in a hydrodynamic sense, and hence this can generate significant variability in their impact on ship performance. Second, the organisms comprising the biofilm produce extracellular polymeric substances (EPS) that make it compliant. This compliancy can produce rich interactions with the fluid flow over the biofilm making flow modeling and drag prediction for biofilm-covered surfaces difficult. Lastly, biofilms can be altered and dislodged by the flow, which makes their drag characteristics time dependent even at a steady flow velocity. Perhaps because of these complexities, there is no generally accepted method for quantifying the nature and impact of a given biofilm, although in recent years more research into biofilms developed on antifouling (AF) paints and FR coatings has been reported (eg Hunsucker et al. 2014; Muthukrishnan et al. 2014; van Mooy et al. 2014; Zargiel & Swain 2014). In spite of recent interest, better guidance is needed to develop a more consistent approach in assessing biofilms. It should be noted that this is related to both identifying critical biofilm parameters and modeling their effects on hydrodynamics.

Despite the aforementioned challenges, a significant body of research has been devoted to quantifying the effect of biofilms on frictional drag. Discussion of the

*Corresponding author. Email: mschultz@usna.edu

The work of M. P. Schultz, C. N. Steppe, and K. A. Flack was authored as part of their official duties as Employees of the United States Government and is therefore a work of the United States Government. In accordance with 17 USC. 105, no copyright protection is available for such works under US Law. J. M. Walker hereby waives her right to assert copyright, but not her right to be named as co-author in the article.

© 2015 Taylor & Francis

Downloaded by [US Naval Academy] at 05:19 14 December 2015

drag penalties of slime films on ships dates at least as far back as McEntee (1915). In this work, the increase in drag as a result of slime is anecdotally asserted to be 0.5% per day while a ship is at dock. Obviously, this is an oversimplification in that the drag increase can be expected to be influenced by myriad factors. It does, nonetheless, point to the longstanding recognition that biofilms can significantly increase the drag of ships. Because of this, the topic has been investigated by a number of researchers over the years (eg Benson et al. 1938; Watanabe et al. 1969; Lewthwaite et al. 1985; Schultz & Swain 1999; Schultz 2004). All these studies indicate that biofilms generate a significant increase in frictional drag. However, the increase is observed to depend strongly on the fouling type, morphology, biofilm thickness and coverage. Within this body of research, the study of Haslbeck and Bohlander (1992) is particularly noteworthy in that it directly documents the effect of a biofilm on the powering requirements of a ship coated with an ablative AF paint. Through ship powering trials conducted before and after hull cleaning, these authors observed that the biofilm increased the powering requirements of the ship by up to 18% compared with the clean hull condition.

Because of the deleterious impacts of biofouling, a number of coating technologies are aimed at reducing the accumulation of biofouling on ships (Finnie & Williams 2010). For the most part these coatings can be grouped into two categories: AF and FR coatings. AF coatings function by using biocides to control biofouling. FR coatings, on the other hand, contain no biocides but act to reduce the adhesion of fouling on the surface such that hydrodynamic forces can dislodge settled organisms. It is of note that both AF and FR coatings are susceptible to fouling by diatomaceous slimes. For example, Schultz et al. (2011) point out that the typical, in-service hull condition for US Navy destroyers coated with ablative copper AF paint systems is a heavy diatomaceous biofilm. FR coatings, particularly silicone-based hydrophobic coatings, foul readily with diatoms, and these biofilms are particularly tenacious on FR surfaces (Holland et al. 2004; Zargiel & Swain 2014). However, the hydrodynamic impact of biofilms on these surfaces is not well established.

The purpose of the present study was to document the impact of biofilms on the frictional drag of FR coating systems. Specifically, the frictional drag of three modern FR coating systems was documented in the clean, as-applied condition as well as after fouling by diatomaceous slime films for periods of ~3 and 6 months. The present work is notable in that the biofilms were grown under dynamic conditions, and the experiments cover a rather large Reynolds number range. The large Reynolds number range allows the frictional drag behavior of the biofilm to be documented over a range of hydrodynamic flow regimes, which in some cases spans from the hydraulically smooth to the fully rough flow regime. These laboratory-scale frictional data were subsequently scaled up to ship-scale using boundary layer similarity-law scaling to predict the impact of these biofilm-fouled FR coatings on the powering requirements of a mid-sized US Navy ship. Figure 1 presents a schematic of the technical approach employed in the present work. The overarching goal of this research was to develop robust roughness scaling for biofilms such that the hydrodynamic effects of biofilms on ships can be estimated from physical measurements of the biofilm alone without resorting to hydrodynamic measurements. It should be noted that the present results should not be interpreted to represent all biofilms that might be

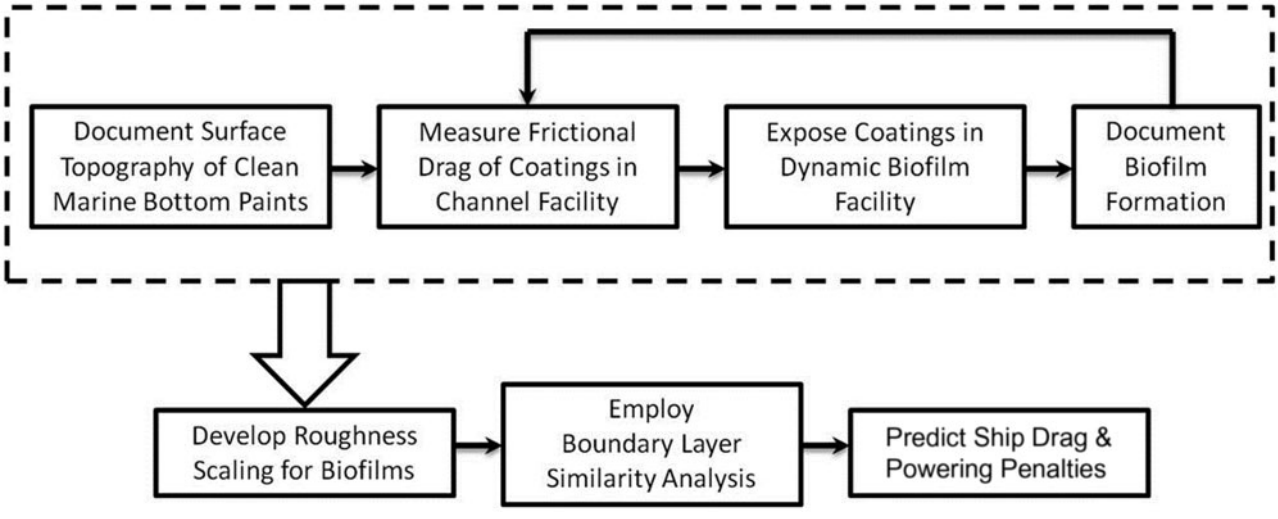


Figure 1. Schematic illustrating the technical approach used in the present study.

found on in-service ships. Instead, they should be taken to be representative examples for the particular biofilm culture reported on here. Further research is needed to explore the effect of the aforementioned complexities of biofilms on the resulting impact on ship performance.

Materials and methods

In this section the experimental facilities and methods will be discussed. First, the turbulent channel flow facility and method used for the hydrodynamic measurements will be presented. Next, the test surfaces used in the present investigation will be discussed. Then some details of the dynamic biofilm exposure facility and method will be given. Finally, the uncertainties associated with the experiments will be examined.

Turbulent channel flow facility and method

The present hydrodynamic experiments were carried out in the high Reynolds number turbulent channel flow facility at the US Naval Academy (USNA) (Figure 2). The test section was 25 mm in height (H), 200 mm in width (W), and 3.1 m in length (L). The channel flow facility had a reservoir tank containing 4,000 l of water. The water temperature was held constant at 22° ± 0.25°C using a thermostat-controlled chiller. The water was deaerated and filtered to remove particulate material >1 µm. The flow was driven by two 7.5 kW pumps operated in parallel. The pumps were operated by separate, variable frequency drive units, which were computer-controlled. The bulk mean velocity in the test section could be varied from 0.4 to 11.0 m s^{-1}. The flow rate was measured using a Yokogawa ADMAG AXF magnetic flowmeter (Yokogawa Electric Corporation, Tokyo, Japan) with an accuracy of ± 0.2% of the reading. The resulting Reynolds number ($Re_m = \bar{U}H/\nu$) based on the channel height (H), bulk mean velocity ($\bar{U}$), and kinematic viscosity of the fluid (ν) spans from 10,000 to 300,000. The resulting wall shear stress (τ_w) ranged from 0.6 to 206 Pa in the facility with smooth walls. This creates wall shear stress conditions that are similar to average conditions on a smooth ship, 150 m in length, travelling at up to 17 m s^{-1} (33 knots). Further details of the facility including flow management devices, tripping, and flow quality are given in Schultz and Flack (2013).

Nine static pressure taps were located in the test section of the channel. They were 0.75 mm diameter holes and were placed along the centerline of the side wall of the channel and were spaced 6.8H apart. The streamwise

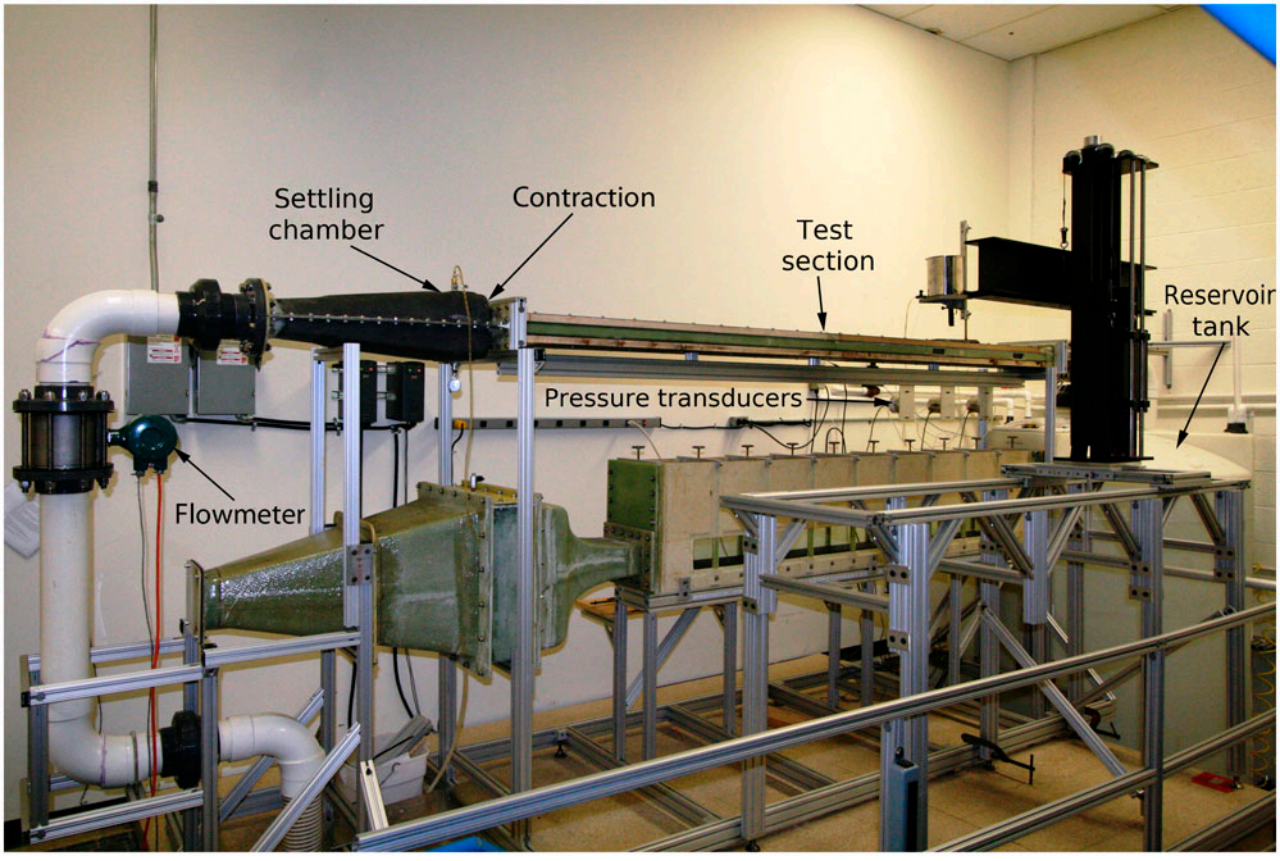


Figure 2. High Reynolds number turbulent channel flow facility at the US Naval Academy.

Downloaded by [US Naval Academy] at 05:19 14 December 2015

Downloaded by [US Naval Academy] at 05:19 14 December 2015

pressure gradient (dp/dx) was determined with three GE-Druck LPM 9,000 series differential pressure transducers (GE Measurement & Control, Billerica, MA, USA). The transducers had ranges of 20, 50, and 100 mbar, respectively, and had an accuracy of ±0.1% of full scale. The use of multiple gauges provided both redundancy in the pressure gradient measurements over their common ranges and also allowed uncertainty to be minimized by using more a sensitive gauge when the pressure gradient was small. Pressure taps 5–8 were used to measure the streamwise pressure gradient in the channel. These were located ~90H–110H downstream of the trip at the inlet to the channel. The linearity in the measured pressure gradient using these four taps was good with a coefficient of determination (R^2) of the regression generally >0.995.

The wall shear stress, τ_w, was determined *via* measurement of the streamwise pressure gradient given as follows:

$$\tau_w = -\frac{H}{2}\frac{\mathrm{dp}}{\mathrm{dx}} \tag{1}$$

or expressed as the skin-friction coefficient, C_f

$$C_f = \frac{\tau_w}{\frac{1}{2}\rho\bar{U}^2} = 2\left(\frac{U_\tau}{\bar{U}}\right)^2 \tag{2}$$

where H = channel height, p = static pressure, x = streamwise distance, ρ = fluid density, $\bar{U}$= bulk mean velocity, and U_τ = friction velocity=$\sqrt{\frac{\tau_w}{\rho}}$.

To obtain the roughness function, ΔU^+, for the test surfaces, the similarity-law procedure of Granville (1987) for fully developed internal flows was employed. Granville's method states that the roughness function can be obtained as follows:

$$\Delta U^+ = \bar{U}_S^+ - \bar{U}_R^+ = \sqrt{\frac{2}{C_{fS}}} - \sqrt{\frac{2}{C_{fR}}} \tag{3}$$

where the subscripts S and R denote smooth and rough surfaces, respectively, evaluated at the same value of the friction Reynolds number (Re_τ) and $^+$ denotes inner normalization (ie by the friction velocity, U_τ, for velocities or by the viscous length scale, ν/U_τ, for lengths). The friction Reynolds number is defined as:

$$Re_\tau = \frac{U_\tau h}{\nu} \tag{4}$$

where h = channel half-height.

In the present study, the flow developed over smooth walls for a distance of 60H in the upstream portion of the channel. The roughness-covered plates formed the top and bottom walls for the remainder of the test section. Guided by the study of Antonia and Luxton (1971), Hong, et al. (2011) found that a fetch of 17.5H downstream of a transition from smooth- to rough-wall channel flow was sufficient to re-establish fully developed conditions in terms of both the mean flow and Reynolds stresses. In the present investigation, there was a roughness fetch of 30H before pressure tap 5, the first tap used in the determination of dp/dx.

In order to confirm that the flow was fully developed, velocity measurements were obtained at locations coinciding with pressure taps 5 and 8 located 90H and 110H, respectively, downstream of the trip. The measurements were made using a TSI FSA3500 two-component laser Doppler velocimeter (LDV) (TSI Inc., Shoreview, MN, USA). Further information about the LDV system is given in Schultz and Flack (2007), and details of the velocity measurements are outlined in Schultz and Flack (2013). Figure 3 shows the mean velocity profiles at Re_τ = 2,000 for a 220-grit sandpaper test surface. Also presented for comparison are the smooth-wall direct numerical simulation (DNS) results of Hoyas and Jimenez (2006) at a similar Re_τ. The collapse of the mean profiles from the two streamwise locations confirms that the flow had become fully developed over this region of the channel. Both of these profiles lie significantly below the smooth-wall DNS results due to an increased momentum deficit as a result of the roughness. Although not shown here, the Reynolds stresses and higher order turbulence statistics measured at the two streamwise locations also show similar agreement (Schultz & Flack 2013).

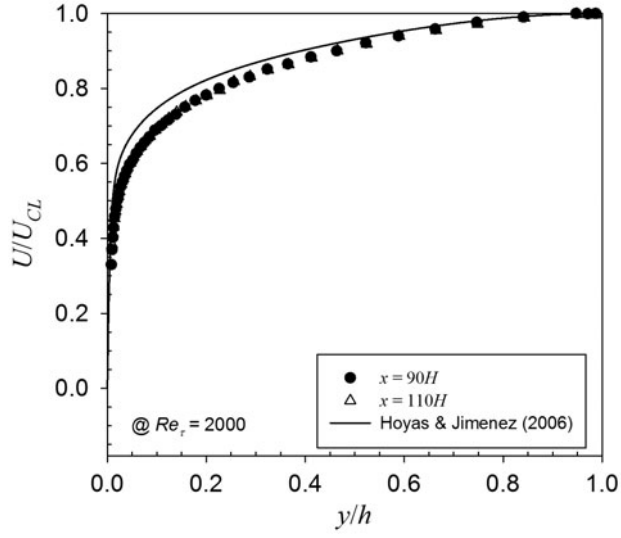


Figure 3. Mean velocity profiles at streamwise locations of x = 90H and 110H for 220-grit sandpaper roughness at Re_τ = 2,000. The velocity, U, is normalized by the centerline velocity, U_{CL}, and the distance from the wall, y, is normalized by the channel half-height, h. The data are compared with the smooth-wall DNS data of Hoyas and Jimenez (2006).

Downloaded by [US Naval Academy] at 05:19 14 December 2015

Test surfaces

The test plates were fabricated from cast acrylic sheet. They were machined using a CNC Haas VF-11 three-axis, vertical milling machine controlled by Esprit CAD/CAM software. The plates were secured to the milling machine by a custom vacuum table fixture. The test plate dimensions were 8.75 mm in thickness, 200 mm in width, and 1.52 m in length. Three commercial FR coating systems were tested: a silicone FR paint system (International Intersleek® 700; Specimen A), a fluoropolymer FR paint system (International Intersleek® 900; Specimen B), and fluoropolymer FR paint system formulated to resist slime fouling (International Intersleek® 1100SR; Specimen C) (International Paint Ltd, Gateshead, UK).

The coatings were applied onto clean and lightly abraded acrylic panels by airless spray at AkzoNobel's Marine Coatings business (International Paint Ltd). All of the coating panels comprised the full coating scheme representative of those typically used on both commercial and military vessels. This included a primer, a tie coat, and a fouling control coating. Following application of the full scheme, all the coated panels were dried for several days at ambient temperature prior to shipment to USNA for testing. Each coating scheme was applied to two replicate test panels. A set of uncoated acrylic control surfaces was also tested.

The surfaces were profiled with a Veeco Wyco NT9100 optical profilometer (Veeco Instruments Inc., Plainview, NY, USA) utilizing white light interferometry. The horizontal resolution of the measurements was 3.5 µm with sub-micron vertical accuracy. Representative images of the surface topography for the three test surfaces are presented in Figure 4. Ten 80 mm long line scans were also collected, which were used to calculate the surface statistics. The profiles were high pass filtered at a cut-off wavelength of 5 mm before calculating the surface statistics. These statistics are presented in Table 1. The results presented are mean values of 20 line scans for each specimen type (two plates per treatment × 10 line scans each). The filtering was carried out because the long wavelength component of the roughness is not expected to contribute significantly to the frictional drag. The 5 mm cut-off used in the present work is similar to that used by Candries et al. (2003). It is worth noting, however, that the selection of the optimum cut-off length in order to characterize a surface in a hydrodynamic sense is still unresolved. A review article by Howell and Behrends (2006) discusses this issue in the context of ship hull paints.

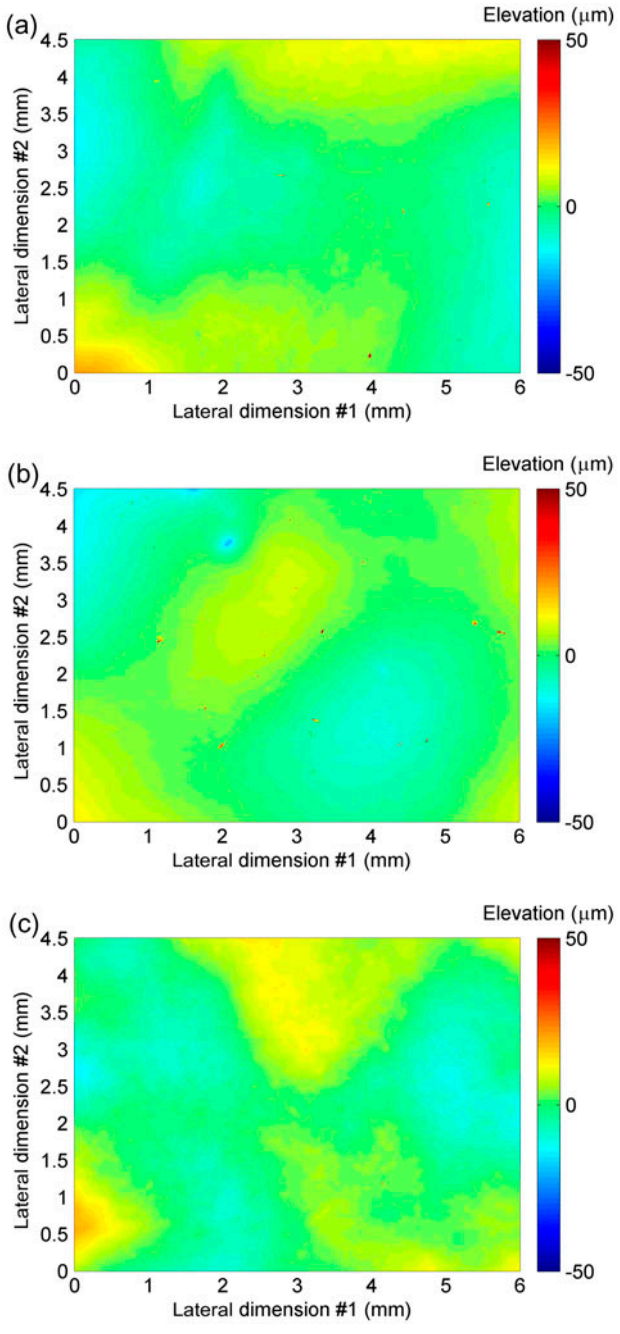


Figure 4. Surface topography maps for: (a) Specimen A; (b) Specimen B; (c) Specimen C.

Table 1. Surface roughness statistics for the FR coating systems tested.

Specimen	R_q (µm)	R_a (µm)	R_t (µm)	R_{sk}	R_{ku}
A	0.53	0.38	2.23	0.57	6.32
B	0.46	0.34	3.03	−0.01	7.65
C	1.22	0.97	4.71	−0.04	3.41

R_q = root-mean-square roughness height; R_a = mean apparent amplitude; R_t = maximum peak-to-trough roughness height; R_{sk} = skewness; R_{ku} = kurtosis. All values are means for 20 measurements per treatment (10 measurements x 2 panels/treatment).

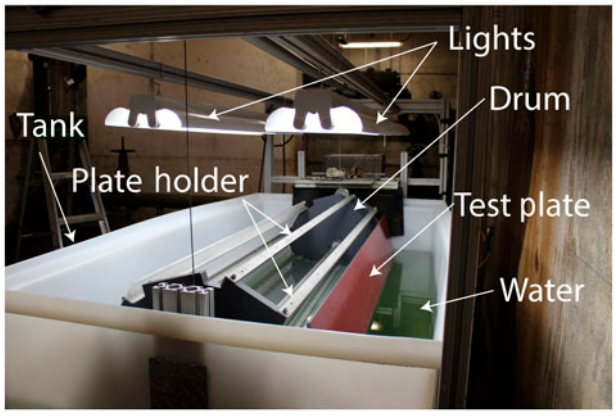


Figure 5. USNA dynamic biofilm exposure facility. Note that drum is elevated above the water surface to illustrate the components of the facility. The top of the drum is 20 cm below the water surface when the facility is operational.

Downloaded by [US Naval Academy] at 05:19 14 December 2015

Dynamic biofilm exposure facility and method

After baseline hydrodynamic tests of the clean coatings, the test surfaces were exposed in the USNA dynamic biofilm exposure facility. The facility, shown in Figure 5, was designed based on ASTM D4939–89 (Standard Test Method for Subjecting Marine Antifouling Coatings to Biofouling and Fluid Shear Forces in Natural Seawater). The test panels were attached to the periphery of a horizontally mounted 61 cm diameter drum that is 1.5 m in length. The drum was horizontally mounted to provide an even distribution of light to the panels. The facility was illuminated by eight fluorescent tubes (95 W each), which were lit for 18 h and dark for 6 h daily. The lighting system was a Sun Blaze® T5 VHO 48 manufactured by Sun System (Vancouver, WA, USA). The facility was kept at a constant temperature of 25° C with a 1 kW heater operated on a thermostat in the tank. The drum, driven by a 0.37 kW AC motor, rotated at a rate of 1 rps producing a peripheral speed of 1.9 m s^{-1} (3.7 knots). The exposure cycle was one week static in the facility followed by three weeks' dynamic exposure. This static/dynamic exposure cycle was repeated for the duration of the exposure period. During the week of static exposure, the drum was rotated ~1/7 of a revolution each day so that all of the specimens received equal amounts of light during that week. The static/dynamic exposure cycle was meant to mimic a conceivable ship operational profile. The facility was filled with 1,700 l of artificial seawater mixed to a salinity of 15 ppt. The tank was inoculated with a diatomaceous biofilm collected from a rubber panel containing 4,5-dichloro-2-n-octyl-4-isothiazolin-3-one (DCOIT). The panel had been exposed in the Indian River Lagoon near Sebastian Inlet, Florida, USA for ~4.5 years. The biofilm included diatoms from four genera: *Amphora*, *Achnanthes*, *Entomoneis* and *Navicula*. All these genera are commonly found in the biofilms on in-service ships (eg Callow 1986; Woods et al. 1986; Hunsucker et al. 2014) and on dynamically exposed AF and FR systems exposed in the marine environment (eg Cassé & Swain 2006; Zargiel & Swain 2014). A volume of ~500 ml of Guillard's F/2 culture medium (Guillard & Ryther 1962) with silicate was added to the biofilm exposure facility weekly.

Before hydrodynamic measurements were made in the turbulent channel flow facility, the test plates were carefully mounted in the channel and exposed to flow. The exposure duration was 15 min, and it was carried out at the maximum velocity used in the hydrodynamic tests. For the plates exposed in the dynamic biofilm exposure facility for 3 months, the maximum bulk mean velocity was 4.4 m s^{-1}. For the plates exposed for 6 months, the maximum bulk mean velocity was 7.5 m s^{-1}. This pre-test exposure allowed loosely attached biofilm to be dislodged before commencing the hydrodynamic measurements.

Representative photographs of the test surfaces taken after hydrodynamic testing for 3 months and 6 months exposure, respectively, are shown in Figures 6 and 7. Five photographs of an area ~200 mm by 300 mm of each of the test surfaces were taken and analyzed with ImageJ image processing software (National Institutes of Health, Bethesda, MD, USA) in order to document the biofilm coverage on the entire test panel. The color threshold and contrast of the images was adjusted with the software such that biofilm-covered portions of the test surfaces could be differentiated from unfouled portions. ImageJ then allowed the biofilm-covered area to be calculated as a percentage of the entire area of the test surface. Measurements of the biofilm thickness were made after hydrodynamic testing using a wet film paint thickness gauge (Model #WF-S; Paul N. Gardner Co., Inc., Pompano Beach, FL, USA). Twenty biofilm thickness measurements were made on each test plate. It should be noted that biofilm thickness measurements were made only on areas of the test surface that had biofilm accumulation. The average biofilm thickness and average percentage coverage on the test surfaces are presented in Table 2. It can be seen from the data in Table 2 that both the biofilm thickness and percentage coverage exhibited a great deal of variation both within and among treatments. To quantify significant differences in biofilm thickness and percentage cover among coating types, Kruskal–Wallis analyses of variance, followed by Tukey's HSD tests were performed in MATLAB v. 2014b (MathWorks, Natick, MA, USA). Data were log-transformed prior to tests, and statistical significance was set to $\alpha = 0.05$.

Ten replicate 25 mm by 25 mm samples were taken from the test panels both before and after hydrodynamic testing. Sampling locations were selected haphazardly

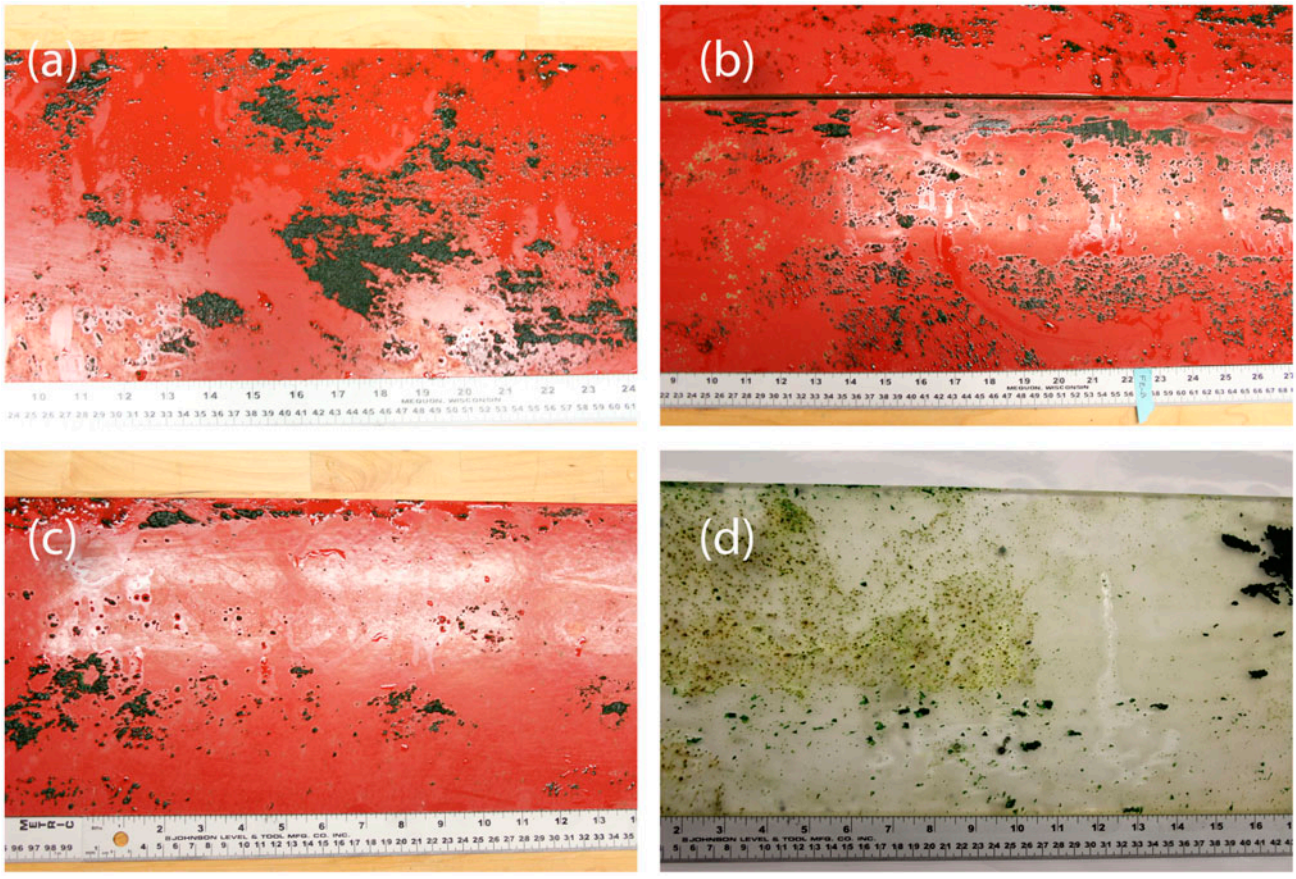


Figure 6. Representative pictures of test surfaces after hydrodynamic testing: (a) Specimen A; (b) Specimen B; (c) Specimen C; (d) Acrylic control. Specimens were exposed in dynamic biofilm exposure facility for 3 months.

along the full length of each panel. The biofilm was scraped from the panels and preserved in 70% EtOH. One milliliter of each well-mixed sample was then added to a Sedgwick rafter cell for taxonomic identification with a compound microscope. While the number of organisms present was reduced after hydrodynamic testing, the species assemblages were largely similar. All the samples collected contained the taxa with which the facility was initially inoculated, namely species of *Amphora*, *Achnanthes*, *Entomoneis* and *Navicula*.

Experimental uncertainty analysis

Uncertainty estimates in the measured quantities presented in this paper were calculated using the method of Moffat (1988), which accounts for both precision and bias. The precision uncertainty in the skin-friction was calculated at 95% confidence by multiplying the standard error (SE) by the two-tailed t value as described in Coleman and Steele (1995). The SEs were calculated from the results of six replicate experiments covering the entire Reynolds number range. Bias estimates were combined with the precision uncertainties to calculate the overall uncertainties in the skin-friction. The overall uncertainty in skin-friction coefficient, C_f, is typically ± 8% at the lowest Reynolds number (Re_m=10,000) but rapidly drops to about ± 1.2% for $Re_m \geq 40{,}000$. The uncertainty in the roughness function was calculated using typical error propagation techniques. The uncertainties in C_f outlined above were propagated through Equation 3. The resulting overall uncertainty in ΔU^+ is ±3.8% or ±0.15, whichever is greater.

Results and discussion

Baseline skin-friction data

The skin-friction coefficient, C_f, results for the clean, unexposed FR surfaces are presented in Figure 8. As can be observed in the three plots, the skin-friction results for the FR surfaces agree within experimental uncertainty with the smooth wall at the low to moderate Reynolds number range. Specimens A (Figure 8a) and B (Figure 8b) begin to show skin-friction that is measurably higher than the smooth wall at $Re_m > 235{,}000$. At the highest

Downloaded by [US Naval Academy] at 05:19 14 December 2015

Downloaded by [US Naval Academy] at 05:19 14 December 2015

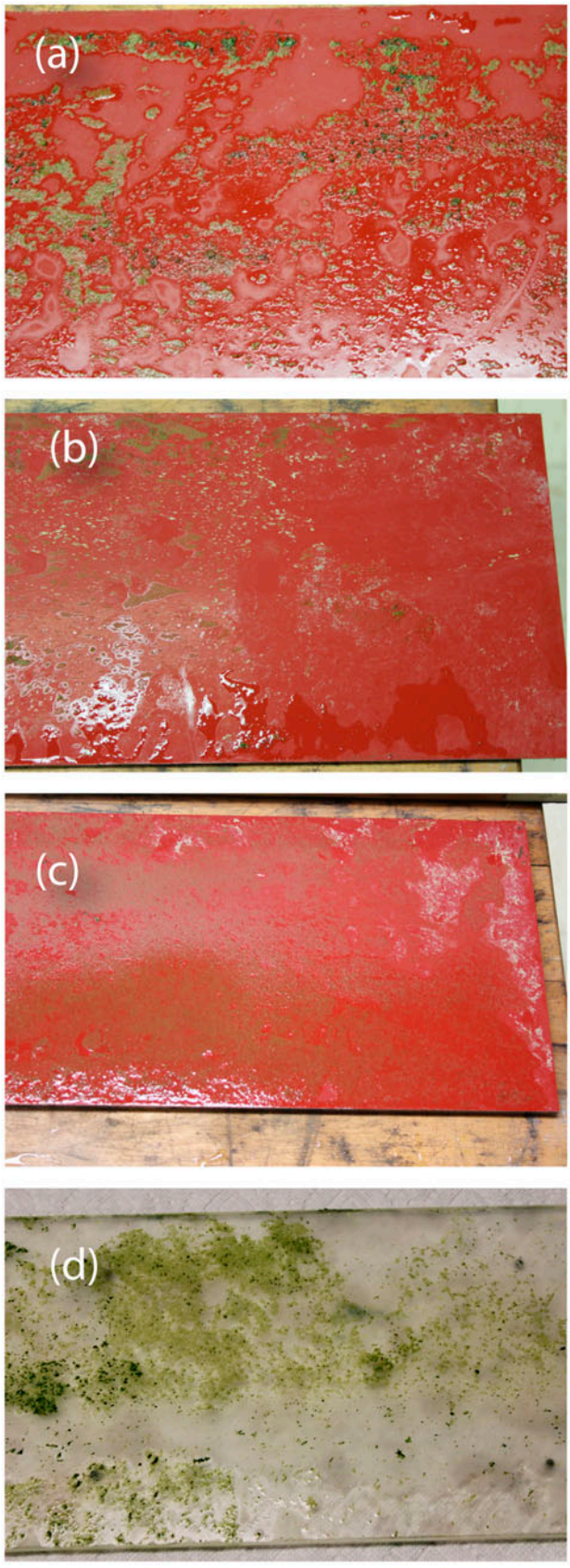


Figure 7. Representative pictures of test surfaces after hydrodynamic testing: (a) Specimen A; (b) Specimen B; (c) Specimen C; (d) Acrylic control. Specimens were exposed in dynamic biofilm exposure facility for 6 months.

Table 2. Biofilm thickness and percentage coverage data for the test surfaces.

Specimen	Exposure duration	k (μm) (mean ± 1 SD)	% Cover (mean ± 1 SD)
A	3 Months	545 ± 248	19.6 ± 6.8
B	3 Months	443 ± 113	11.8 ± 4.7
C	3 Months	574 ± 157	6.4 ± 3.7
Acrylic control	3 Months	527 ± 242	18.1 ± 12.2
A	6 Months	520 ± 100	14.2 ± 8.2
B	6 Months	443 ± 139	13.7 ± 7.8
C	6 Months	98 ± 31	49.2 ± 10.1
Acrylic control	6 Months	392 ± 73	27.8 ± 21.9

The biofilm thickness data are the means and standard deviations for 20 measurements per treatment (10 measurements x 2 panels/treatment). The measurements were only taken on portions of the test panels covered with biofilm. The percent coverage data are the means and standard deviations for 10 images per treatment (5 images x 2 panels/treatment).

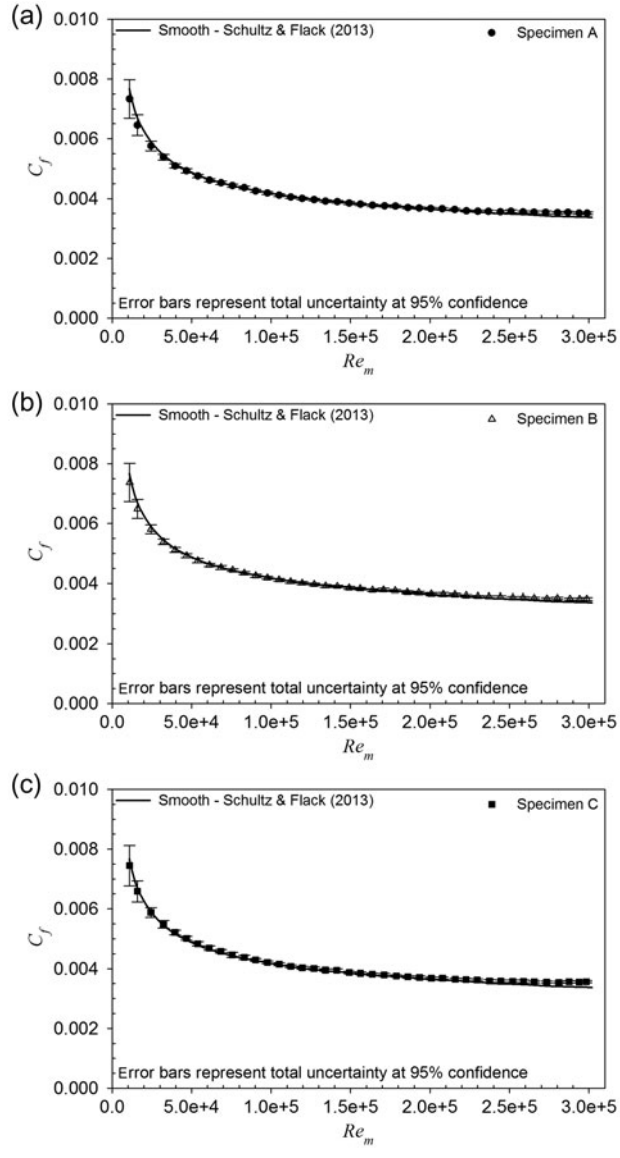


Figure 8. Baseline skin-friction coefficient, C_f, *vs* Reynolds number, Re_m, for the clean, FR surfaces prior to biofilm exposure: (a) Specimen A; (b) Specimen B; (c) Specimen C. The error bars represent the overall uncertainty at 95% confidence.

Downloaded by [US Naval Academy] at 05:19 14 December 2015

Reynolds number tested (Re_m ~ 300,000), the skin-friction for Specimen A was 4.2% greater than the hydraulically smooth condition, while it was 3.6% higher for Specimen B. Specimen C (Figure 8c) started to show the effects of roughness at a slightly lower Reynolds number than the other two coatings. For example, the skin-friction for Specimen C became detectably higher than the smooth wall at Re_m > 210,000 and is 5.7% greater than the hydraulically smooth condition at the highest Reynolds number tested. Overall, the hydrodynamic performance of all the FR surfaces tested in the clean condition is quite similar. The very subtle differences appear to be related to small differences in surface roughness that likely arise from application rather than being inherent in any differences in the coatings themselves. As will be discussed later, all these surfaces would be expected to operate in the hydraulically smooth regime, or nearly so, at ship-scale. It is of note that the paint application used here, while being similar in equipment and technique to that carried out in dry dock, was done in a laboratory setting. This allowed environmental factors to be much more closely controlled and resulted in a smoother paint application. The resulting paint roughness is, therefore, significantly smoother than typically achieved in dry dock (International Paint, personal communication with authors, 3 July 2014). The surfaces presented here should, therefore, be taken as a substantially better finish than can be expected with the given paint system in an actual hull application.

Fouled skin-friction data

The skin-friction results for the FR surfaces after exposure for 3 months to biofilms are presented in Figure 9. All the surfaces tested showed the onset of roughness effects at a fairly low Reynolds number. For example, a significant increase in the skin-friction was observed for all the tests surfaces at Re_m > 30,000. The largest increase is noted for Specimen A and the acrylic control whose skin-friction values agree within experimental uncertainty over the entire Reynolds number range. At the highest Reynolds number tested (Re_m ~ 110,000), the increase in C_f for these surfaces amounts to 33% compared with the smooth wall. The increases in skin-friction observed for Specimens B and C are less than for the other two surfaces. At the highest Reynolds number, the skin-friction for Specimen B was 26% higher than the smooth wall, while it was 14% higher for Specimen C. Specimen C had a significantly lower percentage biofilm cover than specimens A and the acrylic control (p = 0.002). It is worth noting that all the surfaces tested exhibited decreasing C_f with increasing Reynolds number. This is indicative of surfaces that have not yet reached the fully rough flow regime. This could be a result of the maximum Reynolds number of these tests being too low to achieve fully rough behavior. However, as will be seen below for the 6 month biofilm exposure data that were tested at significantly higher Reynolds numbers, this might not be the case and could be indicative of a fundamental change in flow regimes.

The skin-friction results for the FR surfaces after exposure for 6 months to biofilms are shown in Figure 10. Specimens A and B as well as the acrylic control demonstrate an onset of roughness effects at a low Reynolds number (Re_m of at most 22,000). For Specimen C, this onset was delayed to Re_m > 44,000. Some other interesting behavior in the skin-friction can be seen for the four surfaces tested. At low Reynolds number, Specimen A had the highest skin-friction. However, C_f for this surface dropped with Reynolds number such that at the highest Reynolds number (Re_m ~ 190,000) the increase in skin-friction was 65% compared with the smooth wall while the increase seen for the acrylic control was 70%.

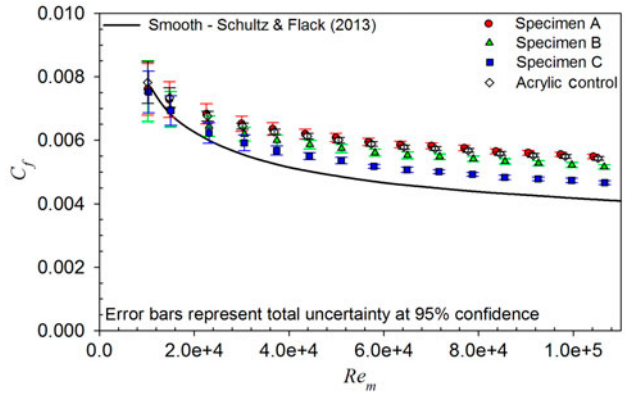


Figure 9. Skin-friction coefficient, C_f, *vs* Reynolds number, Re_m, for the test surfaces after 3 months exposure to biofilms. The error bars represent the overall uncertainty at 95% confidence.

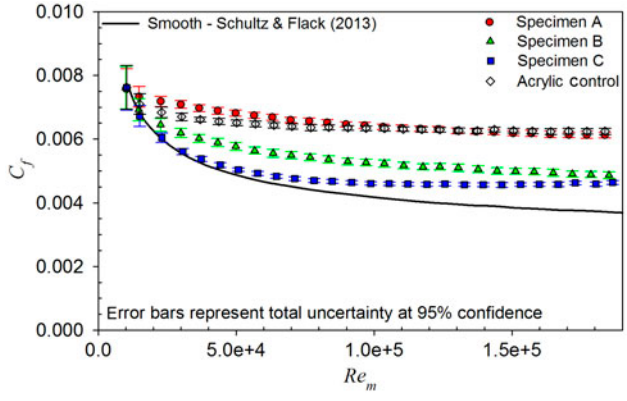


Figure 10. Skin-friction coefficient, C_f, versus Reynolds number, Re_m, for the test surfaces after 6 months exposure to biofilms. The error bars represent the overall uncertainty at 95% confidence.

Downloaded by [US Naval Academy] at 05:19 14 December 2015

Specimen C is observed to have the smallest increase in C_f amongst the surfaces tested. At the highest Reynolds number this was about 25%. Specimen C had the thinnest biofilm of all the treatments ($p < 0.001$), and a significantly higher percentage coverage than Specimens A and B ($p < 0.001$). Another interesting observation can be made regarding the friction curves for the biofilm-covered surfaces in Figure 10. Specimen C and the acrylic control display fully rough behavior. That is, C_f becomes independent of Reynolds number as the Reynolds number became large. Specimens A and B do not display typical fully rough behavior at least over the range of Reynolds number tested here. Instead, C_f continues to drop with Reynolds number over the entire Reynolds number range.

The skin-friction results for the biofilm-covered surfaces taken in their entirety exhibit an interesting trend. The display of fully rough flow behavior, or lack thereof, appears to be more strongly related to the percentage coverage of the biofilm on the test surface than to the biofilm thickness. It can be seen that only surfaces with a mean biofilm coverage of >25% display fully rough frictional behavior. Those with less coverage do not. Therefore, there appears to be a fundamental flow regime change that occurs for a surface with low biofilm coverage. The fully rough flow regime is indicative of a surface whose drag results almost entirely from form drag on the roughness with viscous shear stress becoming negligible. Hence, a lack of Reynolds-number dependence in the skin-friction coefficient may be observed. It would appear that when the percentage coverage is less than ~25% the viscous shear stress on the clean areas of the surface contributes to the skin-friction even at a relatively high Reynolds number. It should be noted that this phenomenon might not be expected to occur on surfaces with elevated baseline roughness. The present surfaces in the baseline condition, however, were hydraulically smooth over the Reynolds number range for which the biofilm hydrodynamic tests were carried out.

Roughness function results and roughness scaling

To this point, discussion has centered on the impact of biofilms on the skin-friction in the turbulent channel flow facility. From a practical perspective what is sought is the effect of these surfaces on the performance of a ship. The percentage increases in skin-friction coefficient discussed previously are not directly indicative of the drag and powering penalties that would result on a ship. However, the roughness function allows these laboratory results to be related to ship-scale. The roughness function, ΔU^+, is the downward shift in the mean velocity profile resulting from the surface roughness. In the present study, it was found using Equation 3. The roughness function is particularly useful because it allows the investigator to relate roughness effects from disparate types of wall-bounded turbulent flows (Schultz and Myers 2003). In the present case, it allows the results from fully developed internal flow (eg turbulent channel flow) to be related to an external flow (eg turbulent boundary layer on a ship).

The roughness function results for the baseline, unfouled coatings are presented in Figure 11. The roughness function is plotted *vs* the roughness Reynolds number based on the root-mean-square roughness height of the coatings, R_q. The choice of this length scale is somewhat arbitrary, and it can be seen in the figure that R_q does not collapse the results from the three coatings. It can be observed, however, that the roughness functions for the coatings display a similar shape and remain relatively small, $\Delta U^+ < 0.8$, over the entire Reynolds number range. It should be noted that a range of possible roughness scaling was employed (eg R_t, R_a), but no length scale was identified to be satisfactory in collapsing the present results to a single curve. Relating the roughness topography to the hydraulic length scale of the clean coating systems remains elusive, and this implies that predicting the hydrodynamic performance of the clean coating systems at ship-scale will require laboratory hydrodynamic tests until this connection can be made.

The roughness function results for biofilm-covered surfaces are presented in Figure 12. The roughness function is plotted versus the roughness Reynolds number based on the mean biofilm thickness, k. Two things are clear from these results. First, it can be seen that k alone is not sufficient to collapse the roughness functions for the biofilm-covered surfaces. Furthermore, the shape of the roughness function is observed to vary significantly

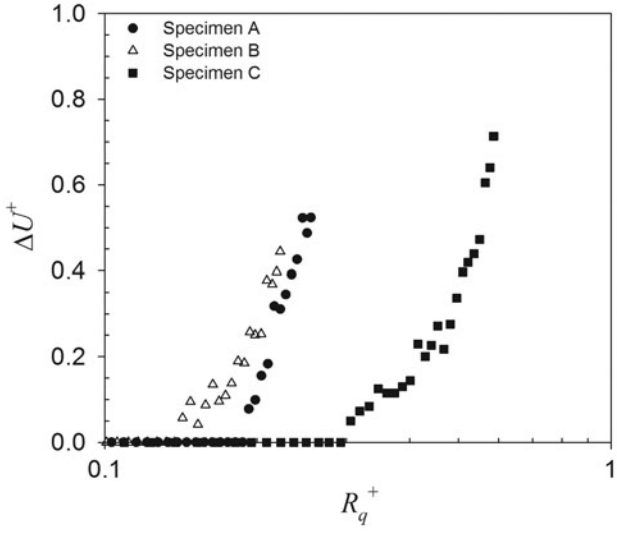


Figure 11. Baseline roughness function, ΔU^+, *vs* roughness Reynolds number, R_q^+, for the clean, FR surfaces prior to biofilm exposure. The overall uncertainty in ΔU^+ is ±3.8% or ±0.15, whichever is greater.

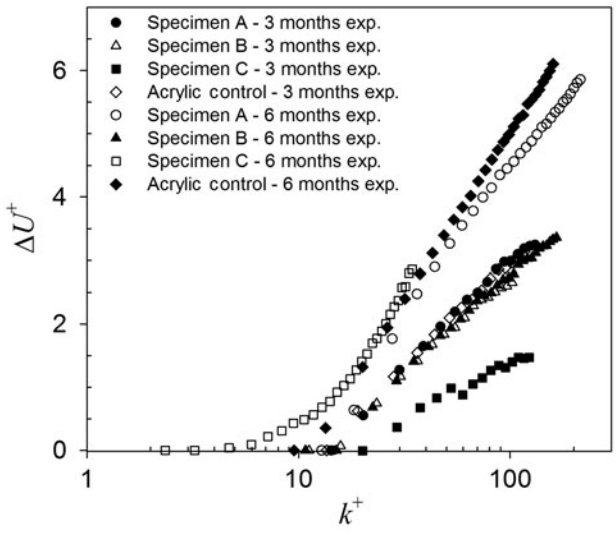


Figure 12. Roughness function, ΔU^+, versus roughness Reynolds number, k^+, for the biofilm-covered test surfaces. The overall uncertainty in ΔU^+ is ±3.8% or ±0.15, whichever is greater.

among the surfaces tested. In order to gain further insight into the roughness function behavior for the biofilm-covered surfaces, the results will be separated into those surfaces that reach the fully rough regime and those that do not.

An equivalent sand roughness height, k_s, can be calculated for the biofilm-covered surfaces that attain fully rough behavior. k_s is the effective roughness length scale of the surface of interest that gives the same roughness function as the uniform sand roughness used in the experiments of Nikuradse (1933). It therefore provides what Bradshaw (2000) terms a 'common currency' among disparate roughness types. Using roughness function data in the fully rough regime, k_s can be calculated using the following relationship:

$$\Delta U^+ = \frac{1}{\kappa}\ln\left(k_s^+\right) - 8.5 + B \qquad (5)$$

where κ= von Kármán constant, k_s^+ = roughness Reynolds number based on the equivalent sand roughness height, and B = smooth-wall log-law intercept. Here κ is taken to be 0.40 and B is 5.0 based on the smooth-wall channel flow results of Schultz and Flack (2013). The skin-friction curves of Specimen C and the acrylic control after exposure for 6 months both display fully rough behavior. The corresponding equivalent sand roughness heights for these surfaces are 35 μm and 115 μm, respectively. Schultz (2007) gives the equivalent sand roughness height for 'light slime' fouling to be 100 μm and 300 μm for 'heavy slime' fouling. The condition of the acrylic control after exposure for 6 months could be characterized as 'light slime' while the condition for specimen C after 6 months exposure might be thought of as 'very light slime' owing to the very thin biofilm (<100 μm). So the present results are in line with those given by Schultz (2007). It should be noted that the values given by Schultz (2007) were based on towing tank tests of statically exposed plates (Schultz 2004). The biofilms developing on these statically exposed plates had a tendency to be thicker with more uniform coverage than the present biofilms grown under dynamic conditions. Some discussion of how this could affect the resulting equivalent sand roughness height is offered below.

The question arises as to how the hydraulic length scale or equivalent sand roughness height, k_s, relates to the biofilm-covered surface. As has been pointed out previously, if such a connection can be made, the hydrodynamic performance of these surfaces at ship-scale can be predicted using physical measurements of the rough surface alone without the need for laboratory-scale hydrodynamic testing. Various attempts to correlate k_s with the physical nature of the surface were made using a range of parameters. These parameters included the mean, root-mean-square, and maximum biofilm thickness as well as the percentage biofilm coverage. The most successful of these employs the mean biofilm thickness and the percentage biofilm coverage. Based on these parameters and the results for the fully rough surfaces, a correlation was developed for what is referred to as the effective roughness length, k_{eff}. k_{eff} is an estimate of k_s based on the mean biofilm thickness and the percentage biofilm coverage. It is given as follows:

$$k_s \approx k_{eff} = 0.055k(\%\text{ biofilm coverage})^{\frac{1}{2}} \qquad (6)$$

It is of note that this correlation is similar in form to one offered by Schultz (2004) for barnacle fouling despite the obvious differences in these fouling types. The roughness function, ΔU^+, results for the fully rough FR surfaces are presented in Figure 13. In this figure, the data are plotted *vs* the roughness Reynolds number based on the effective roughness length, k_{eff}. As can be seen in the figure, k_{eff} causes the roughness function for both surfaces to approach the fully rough asymptote (Equation 5) at large roughness Reynolds numbers indicating that k_s is well estimated by k_{eff}. While there are some differences noted in the roughness function shape for the two surfaces, the onset of roughness effects is observed for both at $k_{eff}{}^+ = 2$–3.

Finally, the roughness function results for the biofilm-covered surfaces that did not reach the fully rough flow regime will be presented. These results are seen in Figure 14. Since k_s for these surfaces could not be calculated, k_{eff} is used as the roughness length scale. It can be seen that k_{eff} is not effective in collapsing the roughness function for all of these surfaces. It appears, however, that this is largely due to the three distinct roughness

Downloaded by [US Naval Academy] at 05:19 14 December 2015

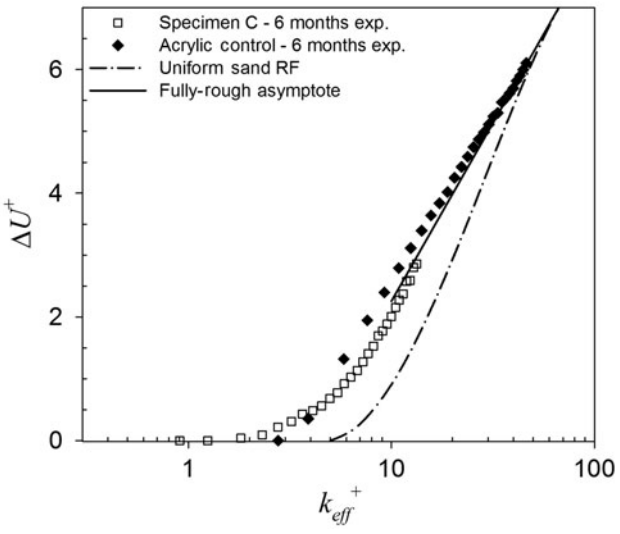


Figure 13. Roughness function, ΔU^+, *vs* roughness Reynolds number, k_{eff}^+, for the biofilm-covered test surfaces that reach the fully rough regime. The solid line is the fully rough asymptote (Equation 5), and the dashed line is the roughness function for uniform sand based on the results of Nikuradse (1933). The overall uncertainty in ΔU^+ is ±3.8% or ±0.15, whichever is greater.

function shapes that are displayed by these biofilm-covered surfaces rather than a shortcoming in k_{eff} as a scaling parameter. For example, the onset of roughness effects for all these surfaces is seen to occur at $k_{eff}^+ = 2$ – 3. Furthermore, k_{eff} is successful in collapsing the results for four of the biofilm-covered surfaces. In addition, although Specimen A/6 months exposure is not technically fully rough, k_{eff} does cause the roughness function for this surface to approach the fully rough asymptote at large roughness Reynolds numbers. All these observations as well as the results for the fully rough surfaces presented in Figure 13 appear to indicate the merit of k_{eff} as a scaling parameter for biofilm-covered surfaces. However, it should be noted that no definitive conclusion in this regard can be made due to the small sample size and the relatively large variability in the thickness and percentage coverage data.

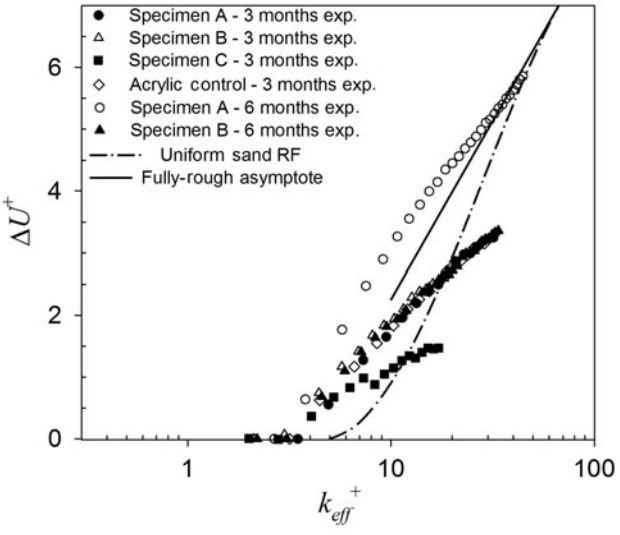


Figure 14. Roughness function, ΔU^+, *vs* roughness Reynolds number, k_{eff}^+, for the biofilm-covered test surfaces that do not reach the fully rough regime. The solid line is the fully rough asymptote (Equation 5), and the dashed line is the roughness function for uniform sand based on the results of Nikuradse (1933). The overall uncertainty in ΔU^+ is ±3.8% or ±0.15, whichever is greater.

The three distinct roughness function shapes that are seen in Figure 14 are worth further discussion. The primary observation is that none of the surfaces displays a roughness function slope tending to κ^{-1} at large roughness Reynolds numbers as is typically expected for fully rough behavior. It is interesting to note that this occurs for the surfaces with the lowest coverage of biofilm. It is possible that for surfaces on which the biofilm coverage is <25%, the flow in the patches between the islands of biofilm relaxes to a state more similar to that on a smooth wall in which viscous shear stress is appreciable even at large Reynolds numbers. There is no clear trend in the roughness function slope and the percentage biofilm coverage that is observed for these surfaces. For example, the surface most closely approaching an asymptotic slope of κ^{-1}, Specimen A/6 months exposure, has a relatively low mean biofilm coverage (14.2%) whereas Specimen A/3 months exposure has a higher coverage (19.6%) but a smaller roughness function slope. However, the surface with the lowest roughness function slope, Specimen C/3 months exposure, does also have the lowest mean biofilm coverage (6.4%). Therefore, for the biofilms tested here, the percentage coverage appears to be a parameter that exerts a significant influence on the fundamental behavior of the roughness function, and it along with the mean biofilm height is important in scaling the biofilm effect.

Effect of paint roughness and diatomaceous biofilms on ship-scale powering

In order to estimate the effect of the paint roughness and biofilms on the powering requirements of a ship, the procedure detailed in Schultz (2007) was used. This method is based on the similarity-law boundary layer scaling of Granville (1958, 1987). Granville's scaling assumes similarity between the mean velocity profiles over smooth and rough walls when expressed in velocity-defect form. This similarity has been established experimentally in both fully developed internal flow (Shockling et al. 2006) and external turbulent boundary layer flow (Connelly et al. 2006). Here, similarity-law boundary layer scaling

Downloaded by [US Naval Academy] at 05:19 14 December 2015

is carried out for the Arleigh Burke-class destroyer (DDG-51). The ship is a mid-sized naval surface combatant with a length of 142 m and a displacement of 8,768 metric tonnes. Further details of the ship are given in Schultz et al. (2011). The powering analysis was made at a ship speed of 7.7 m s^{-1} (15 knots), which corresponds to cruising speed for the vessel. The resulting percentage increases in required shaft power (% ΔSP) values for the various coating conditions are presented in Table 3. It should be noted that the % ΔSP values are taken with reference to the hydraulically smooth condition.

All of the surfaces tested were hydraulically smooth in the unfouled condition at this ship speed and therefore show no increase in required shaft power in this condition. Schultz et al. (2011) suggest ΔSP = 1% for typical AF coatings. However, as noted previously, the present coatings are significantly smoother than generally achieved in dry dock. The biofilm-fouled results show some interesting trends. For example, the silicone-based FR coating (Specimen A) had similar powering penalties to the uncoated acrylic control for both 3 and 6 months exposure in the dynamic biofilm exposure facility. The exposed fluoropolymer FR surfaces (Specimens B and C) showed powering penalties that are significantly lower, with Specimen C having the smallest powering penalties. The present results indicate that the powering penalties expected to result from these biofilms range from 1.5% to 10.1%. Schultz et al. (2011) give the powering penalty for 'light slime' to be 9% and 'heavy slime' to be 18%. The present biofilms would probably best be characterized as 'very light slime' to 'light slime'. Due to the wide range of biofilm coverage and thickness that can exist, characterizing slime layers using terms such as 'very light', 'light', or 'heavy' is probably not most effective in a hydrodynamic sense. Instead it is suggested that a parameter like the effective roughness length, k_{eff}, that is proposed in the present work more faithfully represents the hydrodynamic effect of a biofilm. The reader should be cautioned, however, that the ship powering penalties presented in this work are specific to these particular coatings with a particular roughness on a particular hull form with a particular type and extent of biofilm fouling grown under laboratory conditions. As such, they may not necessarily quantitatively reflect the impact that these coatings will have on any generic, real-world vessel. It is also of note that the present results for the silicone FR surfaces are in line with the previous frictional drag measurements of Swain et al. (2007).

Table 3. Change in required shaft power for a DDG-51 destroyer at 7.7 m s^{-1} (15 knots).

Specimen	Exposure duration	% ΔSP
A	Unexposed	0
B	Unexposed	0
C	Unexposed	0
Acrylic control	Unexposed	0
A	3 months	6.3
B	3 months	4.8
C	3 months	1.5
Acrylic control	3 months	6.2
A	6 months	10.1
B	6 months	5.3
C	6 months	2.3
Acrylic control	6 months	10.1

The change is with respect to the hydraulically smooth condition.

Conclusion

A method to grow diatomaceous biofilms under dynamic conditions and assess their impact on frictional drag has been presented. The results indicate that biofilms can significantly increase the skin-friction of FR surfaces. The effect, however, was quite variable and was observed to depend on both the biofilm thickness and percentage coverage. In the present work, there was some success in scaling the resulting biofilm hydrodynamic impact based on these parameters. However, the ability to predict the impact of a given biofilm on frictional drag based on its physical nature remains far from well understood. It is hoped that future work based on a methodology similar to that outlined here may make more headway in this regard. Especially promising are new techniques to carry out measurements of the biofilm topography *in situ*. These techniques along with detailed measurements of the flow interacting with the biofilm may lead to better understanding and prediction of drag over these surfaces.

Definitions

C_f	skin-friction coefficient = $\frac{\tau_w}{\frac{1}{2}\rho\bar{U}^2}$
h	channel half-height
H	channel height
k	roughness height
k_{eff}	effective roughness height of biofilm
k_s	equivalent sand roughness height
L	channel length
p	static pressure
R^2	coefficient of determination
R_a	mean roughness amplitude
R_{ku}	kurtosis of the roughness profile
R_q	root-mean-square roughness height
R_{sk}	skewness of the roughness profile
R_t	peak-to-trough roughness height
Re_m	Reynolds number = $\bar{U}H/\nu$
Re_τ	friction Reynolds number = $\frac{U_\tau h}{\nu}$
ΔSP	change in required shaft power
U	mean streamwise velocity
$\bar{U}$	bulk mean velocity
U_{cl}	mean streamwise velocity at channel centerline

Downloaded by [US Naval Academy] at 05:19 14 December 2015

U_τ	friction velocity = $\sqrt{\frac{\tau_w}{\rho}}$
ΔU^+	roughness function = $\bar{U}_S^+ - \bar{U}_R^+ = \sqrt{\frac{2}{C_{fS}}} - \sqrt{\frac{2}{C_{fR}}}$
W	channel width
x	streamwise direction
y	wall-normal direction
α	statistical significance level
κ	von Karman constant
ν	kinematic viscosity
r	fluid density
τ_w	wall shear stress
Superscripts	
$+$	normalized by U_τ or V/U_τ
Subscripts	
r	rough wall
s	smooth wall

Acknowledgements

Thanks go to International Paint (IP) for applying the coatings tested in this study. The authors are especially indebted to Barry Kidd, Harry Joyce, Jennifer Longyear, and Phil Stenson from IP who provided significant technical assistance. Kelli and Travis Hunsucker from Geoff Swain's research group at the Florida Institute of Technology Center for Corrosion were instrumental in setting up the dynamic biofilm facility, and for that the authors are extremely grateful. They would also like to thank Brandon Stanley and Joe Dillard at USNA for fabricating the test plates. Technical support for the tests was provided by Don Bunker, Dan Rhodes, and Bill Beaver of the USNA Hydromechanics Laboratory.

Disclosure statement

No potential conflict of interest was reported by the authors.

Funding

The authors gratefully acknowledge the financial support of this research by the Office of Naval Research [ONR Award # N00014-13-WX-2-0747]. The work was also supported by an Australian Fulbright Scholarship for JMW.

References

Antonia RA, Luxton RE. 1971. The response of a turbulent boundary layer to a step change in surface roughness. Part 1. Smooth to rough. J Fluid Mech. 48:721–761.

Benson JM, Ebert JW, Beery TD. 1938. Investigation in the NACA tank of the effect of immersion in salt water on the resistance of plates coated with different shipbottom paints. NACA Memorandum Report C&R C-S19-1(3).

Bradshaw P. 2000. A note on "critical roughness height" and "transitional roughness". Phys Fluids. 12:1611–1614.

Callow ME. 1986. Fouling algae from 'in-service' ships. Bot Mar. 29:351–357.

Candries M, Atlar M, Mesbahi E, Pazouki K. 2003. The measurement of the drag characteristics of tin-free self-polishing co-polymers and fouling release coatings using a rotor apparatus. Biofouling. 19:27–36.

Cassé F, Swain GW. 2006. The development of microfouling on four commercial antifouling coatings under static and dynamic immersion. Int Biodeterior Biodegrad. 57:179–185.

Coleman HW, Steele WG. 1995. Engineering application of experimental uncertainty analysis. AIAA J. 33:1888–1896.

Connelly JS, Schultz MP, Flack KA. 2006. Velocity-defect scaling for turbulent boundary layers with a range of relative roughness. Exp Fluids. 40:188–195.

Finnie AA, Williams DN. 2010. Paint and coatings technology for the control of marine fouling. In: Dürr S, Thomason JC, editors. Biofouling. Oxford: Wiley-Blackwell; p. 185–206.

Granville PS. 1958. The frictional resistance and turbulent boundary layer of rough surfaces. J Ship Res. 2:52–74.

Granville PS. 1987. Three indirect methods for the drag characterization of arbitrarily rough surface on flat plates. J Ship Res. 31:70–77.

Guillard RR, Ryther JH. 1962. Studies on marine planktonic diatoms. 1. *Cyclotella nana* Hustedt and *Detonula confervacea* (Cleve). Can J Microbiol. 8:229–239.

Haslbeck EG, Bohlander G. 1992. Microbial biofilm effects on drag - lab and field. In: Proceedings of the SNAME Ship Production Symposium. Paper No. 3A-1. Jersey City, NJ: SNAME; 7p.

Holland R, Dugdale TM, Wetherbee R, Brennan AB, Finlay JA, Callow JA, Callow ME. 2004. Adhesion and motility of fouling diatoms on a silicone elastomer. Biofouling. 20:323–329.

Hong J, Katz J, Schultz MP. 2011. Near-wall turbulence statistics and flow structures over three-dimensional roughness in a turbulent channel flow. J Fluid Mech. 667:1–37.

Howell D, Behrends B. 2006. A review of surface roughness in antifouling coatings illustrating the importance of cutoff length. Biofouling. 22:401–410.

Hoyas S, Jimenez J. 2006. Scaling of the velocity fluctuations in turbulent channels up to Ret = 2003. Phys Fluids 18: Article # 011702.

Hunsucker KZ, Koka A, Lund G, Swain GW. 2014. Diatom community structure on in-service cruise ship hulls. Biofouling. 30:1133–1140.

Kempf G. 1937. On the effect of roughness on the resistance of ships. Trans INA. 79:109–119.

Leer-Andersen M, Larsson L. 2003. An experimental/numerical approach for evaluating skin friction on full-scale ships with surface roughness. J Mar Sci Technol. 8:26–36.

Lewthwaite JC, Molland AF, Thomas KW. 1985. An investigation into the variation of ship skin frictional resistance with fouling. Trans R Inst Naval Archit. 127:269–284.

McEntee W. 1915. Variation of frictional resistance of ships with condition of wetted surface. Trans SNAME. 24:37–42.

Moffat RJ. 1988. Describing the uncertainties in experimental results. Exp Therm Fluid Sci. 1:3–17.

Muthukrishnan T, Abed RM, Dobretsov S, Kidd B, Finnie AA. 2014. Long-term microfouling on commercial biocidal fouling control coatings. Biofouling. 30:1155–1164.

Nikuradse J. 1933. Laws of flow in rough pipes. NACA Techn Memorandum 1292.

Schultz MP. 2004. Frictional resistance of antifouling coating systems. ASME J Fluids Eng. 126:1039–1047.

Schultz MP. 2007. Effects of coating roughness and biofouling on ship resistance and powering. Biofouling. 23:331–341.

Schultz MP, Flack KA. 2007. The rough-wall turbulent boundary layer from the hydraulically smooth to the fully rough regime. J Fluid Mech. 580:381–405.

Downloaded by [US Naval Academy] at 05:19 14 December 2015

Schultz MP, Flack KA. 2013. Reynolds-number scaling of turbulent channel flow. Phys Fluids 25:Article #025104.
Schultz MP, Myers A. 2003. Comparison of three roughness function determination methods. Exp Fluids. 35:372–379.
Schultz MP, Swain GW. 1999. The effect of biofilms on turbulent boundary layers. ASME J Fluids Eng. 121:733–746.
Schultz MP, Bendick JA, Holm ER, Hertel WM. 2011. Economic impact of biofouling on a naval surface ship. Biofouling. 27:87–98.
Shockling MA, Allen JJ, Smits AJ. 2006. Roughness effects in turbulent pipe flow. J Fluid Mech. 564:267–285.
Swain G, Kovach B, Touzot A, Casse F, Kavanagh CJ. 2007. Measuring the performance of today's antifouling coatings. J Ship Prod. 23:164–171.
Townsin RL. 2003. The ship hull fouling penalty. Biofouling. 19:9–15.
Van Mooy BAS, Hmelo LR, Fredricks HF, Ossolinski JE, Pedler BE, Bogorff J, Smith PJS. 2014. Quantitative exploration of the contribution of settlement, growth, dispersal and grazing to the accumulation of natural marine biofilms on antifouling and fouling-release coatings. Biofouling. 30:223–236.
Watanabe S, Nagamatsu N, Yokoo K, Kawakami Y. 1969. The augmentation in frictional resistance due to slime. J Kansai Soc Naval Archit. 131:45–53.
Woods DC, Fletcher RL, Jones EBG. 1986. Diatom fouling of in-service shipping with particular reference to the influence of hydrodynamic forces. In: Round FE, editor. Proceedings of the ninth international diatom symposium. Bristol: Biopress; p. 49–59.
Zargiel KA, Swain GW. 2014. Static *vs* dynamic settlement and adhesion of diatoms to ship hull coatings. Biofouling. 30:115–129.

Downloaded by [US Naval Academy] at 05:19 14 December 2015